

Article

Networked Control of Electric Vehicles for Power System Frequency Regulation with Random Communication Time Delay

Yunpeng Guo ¹, Liyan Zhang ², Junhua Zhao ³, Fushuan Wen ^{4,*}, Abdus Salam ⁴, Jianwei Mao ⁵ and Liang Li ⁵

¹ School of Electrical and Electronic Engineering, North China Electric Power University, Beijing 102206, China; guoyunpeng1976@163.com

² School of Electrical Engineering, Zhejiang University, Hangzhou 310027, China; liyan010406@gmail.com

³ School of Science and Engineering, Chinese University of Hong Kong (Shenzhen), Shenzhen 518100, China; zhaojunhua@cuhk.edu.cn

⁴ Department of Electrical and Electronic Engineering, Universiti Teknologi Brunei, Bandar Seri Begawan BE1410, Brunei; abdu.salam@utb.edu.bn

⁵ Division of Electric Vehicle Service, State Grid Zhejiang Electric Power Company, Hangzhou 310007, China; mao_jianwei@zj.sgcc.com.cn (J.M.); liiliang@foxmail.com (L.L.)

* Correspondence: fushuan.wen@gmail.com; Tel.: +673-2461020 (ext. 1316); Fax: +673-2461035

Academic Editor: K.T. Chau

Received: 4 February 2017; Accepted: 13 April 2017; Published: 3 May 2017

Abstract: Electric vehicles (EVs) can have noteworthy impact on power system dynamic performance. This paper develops two novel controllers which can take into account the random time delay in the communication channel of the control system. With the designed robust controller, the system can utilize EVs to participate in automatic generation control (AGC) processes so as to assist conventional thermal power units to respond rapidly and accurately to load fluctuations, as well as to enhance the capability of a power system to accommodate renewable energy forms such as wind power. Owing to the distributed nature of EVs, a networked control scheme for EVs' participation in frequency regulation is first proposed in the paper. A closed-loop block diagram, which incorporates EVs and wind power, is then developed. Two controllers are then designed based on rigorous linear matrix inequalities (LMI) theory to ensure the robustness and stability of the system. Finally, comprehensive case studies based on a two-area equivalent of the IEEE 39-bus test system are performed to demonstrate the effectiveness of the proposed methods.

Keywords: frequency regulation; electric vehicles; wind power; networked control; linear matrix inequalities; optimal H_{∞} -PID full-state feedback control; suboptimal H_{∞} -PID output feedback control

1. Introduction

The conflict between the increasing energy demand and environmental concerns is becoming more and more severe along with the social and economic development of society. Plug-in Electric Vehicles (PEVs) have attracted increasing interest in the past decade due to their environmentally friendly characteristics. The integration of numerous PEVs, including Plug-in Hybrid Electric Vehicles (PHEVs), into the future smart grid may have significant impact on the security and economics of the concerned power system. On the one hand, PEVs consume electricity like traditional loads. On the other hand, with the Vehicle to Grid (V2G) technology [1], a large number of PEVs can be used as controllable energy storage devices to participate in optimum system operation. Moreover, PEVs can also help to stabilize load fluctuations and enhance the ability of the system to accommodate intermittent renewable energy, which has been successfully applied in the Pennsylvania-Jersey-Maryland (PJM) electricity

market in the USA [2]. The report also points out that, “the most economic entry for this green innovation is the market for ancillary services (A/S). The highest value A/S is frequency regulation.”

This paper focuses on the control problem, which is different from the optimal dispatching problem of electric vehicles [3–5]. In the dispatch problem, the time span considered is much longer: i.e., how to arrange the charging/discharging plans an hour or a day ahead to optimize a given objective function, such as to minimize the load fluctuations, network loss or operation costs. In this context, the random behaviors of the charging/discharging time and mileage differences of the PEVs are quite evident and have to be considered. However, in the present PEV control problem, the aim is how to design a controller using advanced control laws, which determine a total charging/discharging power of PEVs in a short period of within 2 min to help to alleviate load fluctuations. In this quite short period, especially during the midnight hours when the wind power fluctuates significantly [1], the number of the participating PEVs can be kept roughly stable by implementing a registration mechanism as well as an appropriate level of compensation, so that the randomness can be less considered and the key point is the small disturbance stability of the whole system itself.

For the PEV control problem, reference [6] proposed a new supplementary Load Frequency Control (LFC) method by using both EVs and Heat Pump Water Heaters as controllable loads, but it did not account for the information delay when using the PI controller. In [7], the possibility that excess energy can be supplied back to the grid for meeting peak demand by using Fuzzy Logic Controller and V2G technology was demonstrated. However, due to the battery degradation cost caused by deep charge/discharge cycles, it might not be economical for EV owners to participate in the electricity market. In [8], the optimal control strategy of distributed EVs under the administration of a centralized EV charging service provider (CSP) was proposed, the problem was then solved using the flow network method. The proposed method could guarantee the electricity grid constraints such as voltage and power flow limits. In [9], a Model-Predictive Control method was proposed to control EVs’ participation in the frequency regulation process. The result demonstrates the effectiveness of clustering large numbers of PHEVs and household appliances.

However, in the existing literature, the communication delay in the PEV control problem was not considered. The previous works assumed that the information received was timely and accurate. This however is not always true in the PEV control problem, especially when the control signal is communicated using a general communication network. In practice, communication delays and data losses are inevitable; and it is widely accepted that the communication delays and data losses could significantly degrade the control system performance. In the PEV control problem, the number of PEVs in the smart grid can be huge, and each EV aggregator needs to exchange information with the control center, thus the data traffic can be very heavy. Unfortunately, conventional power system analysis and control methodologies cannot appropriately address the impacts of the communication system. However, the performance of the communication infrastructure has great impacts on PEV control and must be taken into account properly to solve this typical networked control problem [10].

The rest of this paper is organized as follows: the basic structure of networked control system (NCS) and the framework of using PEVs for frequency regulation are introduced in Section 2. In Section 3, a block diagram of the networked LFC system with PEVs and wind power is developed. In Section 4, two novel control methods, i.e., optimal H_∞ -PID full-state feedback control and suboptimal H_∞ -PID output feedback control are designed based on Linear Matrix Inequalities (LMI) theory. Comprehensive case studies are presented in Section 5 to test the impacts of PEVs and time delay on the control system performance, and verify the effectiveness of the proposed approaches. Section 6 finally presents the conclusions of the paper.

2. Basic Theory of Networked Control System and the Framework of Frequency Regulation with EVs

2.1. General Structure of Networked Control System (NCS)

A networked control system is a system in which the sensor, controller and actuator are connected with a communication network as shown in Figure 1 [10]. In traditional power system analysis, the impacts of the communication network are not taken into account since it is considered perfectly reliable, with a dedicated line for thermal or hydro power plants. However, in the future grid, due to the huge number of PEVs and the distributed EV agents under fierce market competition, it is not practical to build a dedicated line for each one to participate in system operation. The more viable approach is to implement the communication using a general purpose network (e.g., a wireless network/Ethernet/LAN/Internet, etc.). In this case, the problems of communication delay are very likely to occur and it is a typical Networked Control System. The communication delay can degrade the system performance, even cause instability and collapse of the whole power system [11]. Therefore, the effects of communication delay must be taken into account in the analysis and design of smart grid control system for control center.

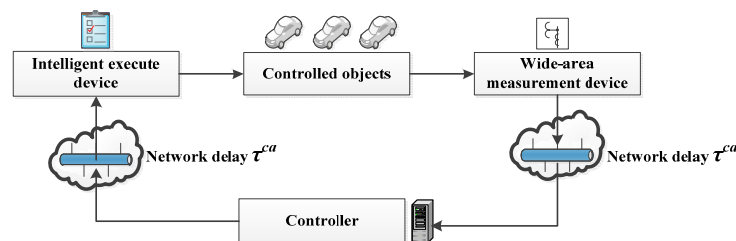


Figure 1. The structure of the networked control system.

2.2. The Advantages of Using PEVs for Frequency Regulation and Implementation Framework

Compared with conventional AGC generators, there are some special merits which make PEV an attractive choice for Load Frequency Control (LFC):

- (1) For AGC plants, the control signal response amplitude and the polarity are strictly limited; while for PEVs, the advanced power electronic devices eliminate this restriction.
- (2) For thermal units, the large adjustment may increase the cost and damage the lifespan. On the contrary, V2G responses rapidly and accurately and has a relatively smaller time constant, therefore, it can reduce the adjustment capacity requirement of the generators.
- (3) Since the battery is in the floating charge state when it participates in ancillary service, compared with the depth charge state when it participates in energy market, the adverse impact on battery's life can be alleviated and the efficiency of the battery can be improved at the same time [12]. Besides, the economic compensation for participating in ancillary service is much more profitable than energy market, thus the drivers tend to register their cars to participate in LFC especially at midnight.

2.3. The Framework of the Networked Frequency Regulation with EVs and Control Process

As shown in Figure 2, due to the large number of the distributed access to the power system, it is appropriate to take a hierarchical approach to control the charge and discharge behaviors of PEVs. It is neither realistic nor necessary for the control center to send control signals directly to each EV. In the work of this paper, we adopt the concept of the electric vehicle aggregator [13]. Each EV aggregator manages a cluster of electric vehicles, and is responsible to report the status information to the control center. It receives the control signals from the control center, and controls the charge/discharge behaviors of its PEVs to implement the control strategies given by the control center.

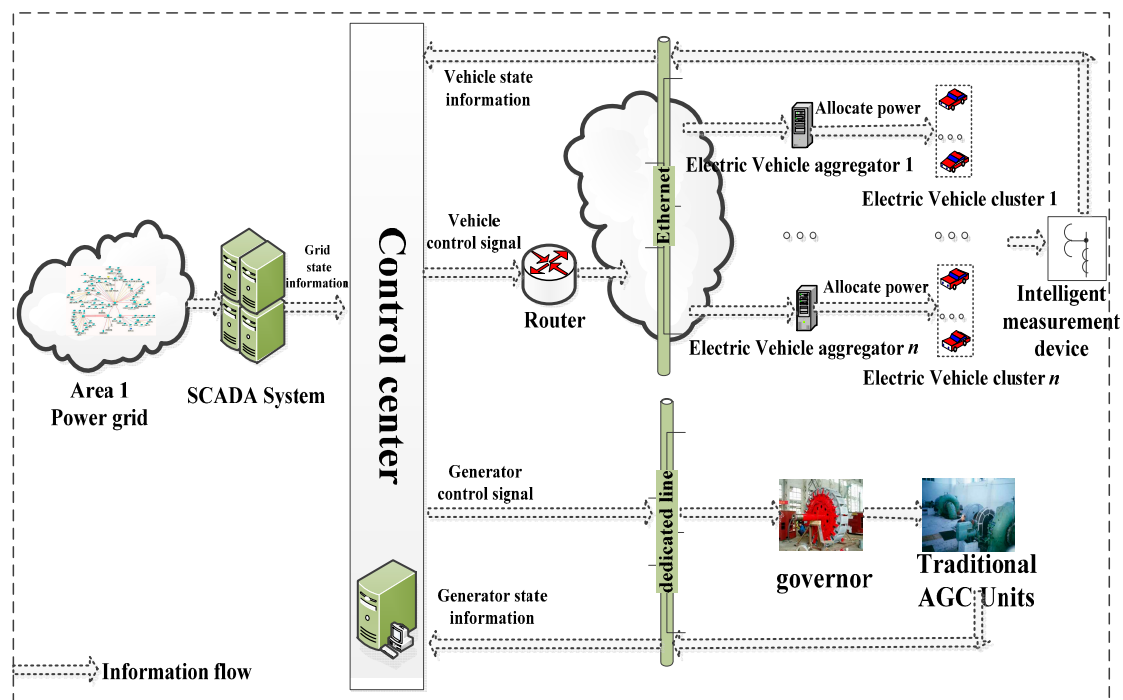


Figure 2. The architecture of a networked frequency regulation system with EVs.

The frequency regulation procedure for the entire power system can be described as follows:

- (1) The control center obtains real-time measured information (frequency, tie-line exchange power, etc.) via the Supervisory Control And Data Acquisition (SCADA) system, and calculates the Area Control Error (ACE);
- (2) Combine ACE, unit status with other vehicle status information, then send real-time control signals obtained with the suboptimal H_{∞} -PID output feedback controller proposed below to AGC plants and EV aggregators;
- (3) The generators participating in frequency regulation respond to load fluctuations according to the control signals;
- (4) EV aggregators determine the charge/discharge power of each PEV based on the received control signals. For example, one of the basic approaches is the proportional allocation method, which is an equilibrium of fairness and efficiency.

Specifically, the EV aggregator firstly inquires the State of Charge (SOC) and calculates the total power of all the vehicles it manages. It then allocates the charging/discharging power based on the following equation:

$$P_{i,t} = \frac{S_{i,t}}{\sum_{k=1}^N S_{k,t}} P_t, \forall t \in T \quad (1)$$

where, $P_{i,t}$ is the charging/discharging power allocated to vehicle i at time t ; P_t is the total output power allocated by the control center to the specific EV aggregator at time t ; $S_{i,t}$ is the SOC of vehicle i at time t ; N is the total number of PEVs that are registered to participate in frequency regulation. How to optimize the allocation of power to each PEV so as to maximize their profit is another important problem for EV aggregators, which is not the emphasis of this paper.

2.4. Analysis of Communication Delay

In the PEV control problem, since the communication will likely be implemented with a general-purpose network, network-induced communication delays will be inevitable. The

communication delays can be divided into propagation delays, switching delays, access delays and queuing delays. An important factor which can influence communication delays is the media access control protocol used by the NCS. Table 1 lists some of the typical access control protocols and their corresponding delay characteristics.

Table 1. Control networks and delay characteristics.

Network	Ethernet	CAN Bus	TP Bus
Access mode	Random access	Random access	Token passing
Network protocol	IEEE 802.3 CSMA/CD	CSMA/AMP	IEEE 802.4
Data packet	Maximum 1500	Maximum 8	Maximum 504
Delay characteristics	Random; Unbounded	Random; Bounded	Random; Bounded; Periodic

The delay characteristics are different in different communication networks. In this research, Ethernet is considered since it is widely used, but the methodology and framework also apply to other communication networks. Although Ethernet has its advantages of high data transfer rates and low power consumption, its drawbacks, however, are also quite obvious. When the communication network is heavily loaded, the time delay is random, which puts a relatively higher requirements for maintaining the stability and robustness of the control method and system.

3. Model of Closed-Loop Frequency Regulation System with PEVs and Wind Power

For the purpose of achieving LFC, a comprehensive model has to be built. Although the single battery model has been thoroughly discussed in quite a few previous works [14,15], it would not be appropriate to consider each of the battery characteristics separately hence a cluster of numerous PEVs as well as traditional generators are controlled together to change their injection power to follow the load disturbances. The distribution of charging/discharging power of each vehicle is another optimization problem which is beyond the main consideration in this paper, however the basic allocation ideas have been presented in Section 2.

A new two-area closed-loop LFC block diagram with PEVs and wind power is developed and shown in Figure 3. All generators and EVs which are under the management of one aggregator are lumped as equivalent modules.

Without the loss of generality, we assume that there is one EV aggregator in each area, and the method proposed is also applicable if more agents are integrated. The networks induced delay $\tau = \tau^{sc} + \tau^{ca}$ exists in the transmission channel [16], from the EV aggregator to the control center. Assuming the Ethernet is used in this problem, the time delay is therefore random and unbounded. In Figure 3, the tie line is denoted with the long dashed line while the controller is represented by the short dashed line. The controller needs to be designed. The model of the closed-loop LFC in Figure 3 is first developed and then three control methods will be presented: the traditional PI control, the proposed optimal H_∞ -PID full-state feedback control and the proposed suboptimal H_∞ -PID output feedback control.

$$\begin{aligned}
 B_1 &= \begin{bmatrix} -\frac{1}{M_1} & 0 & 0 & 0 & 0 & 0 & 0 & 0 & 0 \\ 0 & 0 & 0 & 0 & 0 & -\frac{1}{M_2} & 0 & 0 & 0 \end{bmatrix}^T \\
 B_2 &= \begin{bmatrix} 0 & \frac{K_{SG1}}{T_{G1}} & 0 & 0 & 0 & 0 & 0 & 0 & 0 \\ 0 & 0 & 0 & 0 & 0 & 0 & \frac{K_{SG2}}{T_{G2}} & 0 & 0 \end{bmatrix}^T \\
 B_3 &= \begin{bmatrix} 0 & 0 & 0 & \frac{K_{EV1}K_{SEV1}}{T_{EV1}} & 0 & 0 & 0 & 0 & 0 \\ 0 & 0 & 0 & 0 & 0 & 0 & 0 & \frac{K_{EV2}K_{SEV2}}{T_{EV2}} & 0 \end{bmatrix}^T \\
 C_1 &= \begin{bmatrix} K_{B1} & 0 & 0 & 0 & 1 & 0 & 0 & 0 & 0 \\ 0 & 0 & 0 & 0 & 1 & K_{B2} & 0 & 0 & 0 \end{bmatrix}; \quad D_{11} = D_{12} = \begin{bmatrix} 0 & 0 \\ 0 & 0 \end{bmatrix}
 \end{aligned}$$

where D_i ($i = 1, 2$) is the load frequency characteristic coefficient; M_i , R_i , T_{Gi} and T_{Chi} ($i = 1, 2$) are respectively the inertia time constants of the AGC units, the speed regulation due to governor action, the governor time constant, and the turbine time constant; K_{EVi} and T_{EVi} ($i = 1, 2$) are frequency response coefficients of PEVs and equivalent time constant of the batteries respectively; T is the tie line synchronization coefficient; K_{SGi} and K_{SEVi} ($i = 1, 2$) are capacity distribution coefficients for frequency regulation of AGC units and PEVs, and satisfy $K_{SGi} + K_{SEVi} = 1$ ($i = 1, 2$).

4. Controller Design Based on LMI Theory

4.1. Summary of the LMI Methods

The system cannot work without a suitable controller if it is disturbed or a network-induced delay occurs. A control system can be abstracted as the generalized object $G(s)$ that will be controlled by $K(s)$, the goal of the H_∞ robust control [17] is to design a real regular function controller $K(s)$ to ensure the internal stability of the generalized object. On this premise, the controller has to minimize impacts of the input disturbance, i.e., guarantees the transfer function (from the disturbance input $w(t)$ to control output $z(t)$) $G_{wz}(s)$'s H_∞ norm would not exceed a pre-given small positive constant γ , which means $\|z(t)\|_2 < \gamma \|w(t)\|_2, \forall w \in L_2[0, +\infty)$ under the zero initial condition $x(t) = 0$ ($t \in [-d, 0]$). Here, $\|z(t)\|_2$ is the signal's L_2 norm, which essentially represents the energy of the signal and can be mathematically defined as in [16]: $\|z(t)\|_2 = \|Z(j\omega)\|_2 = \sqrt{\frac{1}{2\pi} \int_{-\infty}^{+\infty} \text{tr}(\hat{Z}^*(j\omega)\hat{Z}(j\omega))d\omega}$, $L_2[0, +\infty)$ denotes a set of the time-domain signals that are L_2 norm bounded and is actually a Hilbert space. The controller obtained is called suboptimal robust H_∞ controller, with γ expresses the capability of the system to suppress the external input interference $w(t)$ and is called "interference suppression degree". A smaller γ indicates better robust performance and stability of the system. An optimal robust H_∞ controller can be obtained by minimizing γ so as to get the smallest value of the interference suppression degree.

In the networked frequency regulation system with PEVs, not only the outside interference vector $w(t) = [w_1 w_2]^T = [\Delta P_{L1} \Delta P_{L2}]^T$ that will undermine the stability of the system, the communication delay also has to be taken into account. Therefore, the H_∞ control method has to be used for time delayed system. In recent years, with the development of the linear matrix inequality (LMI) theory, LMI-based controller design has been successfully applied in practical systems.

4.2. Design of the Full-State Feedback Controller

It is better to design a full-state feedback controller when all system states are measurable, because if more states can be fed back, the system usually will achieve better dynamic performance. Here we propose a novel theorem that can be used to design the full-state feedback H_∞ controller. This controller design method can be generalized for other application situations.

Theorem 1. (due to space limitations, the proof is given in the Appendix A)

For a networked control system (2), if the communication delay satisfies $0 \leq \tau(t) < \infty$, $\dot{\tau}(t) \leq \rho < 1$, (A, B_2, C_1) is stabilized and can be detected [17]; then for a pre-given positive constant γ , we can design a memoryless full-state feedback controller $u(t) = Kx(t)$, if there exist two positive definite matrixes X , and S , as well as a matrix Y such that the following LMI holds:

$$\begin{bmatrix} (AX + B_2Y)^T + AX + B_2Y + S & B_3Y & B_1 & (C_1X)^T \\ (B_3Y)^T & -(1 - \rho)S & 0 & 0 \\ B_1^T & 0 & -\gamma I & 0 \\ C_1X & 0 & 0 & -\gamma I \end{bmatrix} < 0 \tag{3}$$

Then there is a memoryless γ -suboptimal full-state feedback controller $u(t) = Kx(t)$. In particular, if $(\hat{X}, \hat{Y}, \hat{S})$ is a feasible solution of (3), then $u(t) = \hat{Y}\hat{X}^{-1}x(t)$ is one of the γ -suboptimal full-state feedback controllers of the system. Specifically, through solving the optimization problem:

$$\begin{aligned} & \min \gamma \\ & \text{s.t. (3) \& } X > 0 \end{aligned}$$

We can get the optimal full-state feedback H_∞ controller to minimize the interference suppression degree γ . This problem is substantially a semi-definite programming problem that can be solved using LMI Toolbox [18].

4.3. Design of the Output Feedback Controller

If not all the state variables can be measured (e.g., the valve opening degree) or the measurement cost is too high to do so, from the economical perspectives, we need to design output feedback controller instead of the full-state controller at the expense of sacrificing the system dynamic performance to some extent. For system (2), if we define y as the dynamic output-feedback vector, the controller equations can be denoted as:

$$y(t) = C_2x(t) \tag{4}$$

$$\dot{\zeta}(t) = A_k\zeta(t) + B_ky(t) \tag{5}$$

$$u(t) = C_k\zeta(t) + D_ky(t) \tag{6}$$

The H_∞ part of the hybrid controller is depicted in Figure 4:

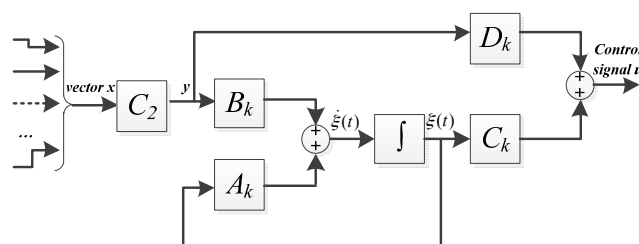


Figure 4. The H_∞ part of the output feedback controller.

Where, $y = [y_1, y_2 \dots \dots y_l]^T \in R^{l \times 1}$ are l -dimension output feedback variables, since we cannot measure all elements of x , we have $l < n$; $\zeta = [\zeta_1 \zeta_2 \dots \dots \zeta_k]^T \in R^{k \times 1}$ are k -dimension controller state variables, k is unknown and undetermined. $A_k \in R^{k \times k}$, $B_k \in R^{k \times l}$, $C_k \in R^{m \times k}$, $D_k \in R^{m \times l}$ are controllers to be designed. Here we propose a novel theorem that can be used to design the output feedback H_∞ controller.

Theorem 2. (due to space limitations, the proof is given in the Appendix B)

For the networked control system that can be expressed as (2) and (4)–(6), the H_∞ output feedback controller $K = \begin{bmatrix} D_k & C_k \\ B_k & A_k \end{bmatrix}$ can be designed with the following definitions and LMIs:

$$\begin{bmatrix} W_1 & 0 & 0 & 0 & 0 \\ 0 & I & 0 & 0 & 0 \\ 0 & 0 & I & 0 & 0 \\ 0 & 0 & 0 & I & 0 \\ 0 & 0 & 0 & 0 & I \end{bmatrix}^T \begin{bmatrix} AX + XA^T & 0 & B_1 & XC_1^T & X \\ 0 & -(1-\rho)Q & 0 & 0 & 0 \\ B_1^T & 0 & -\gamma I & 0 & 0 \\ C_1 X & 0 & 0 & -\gamma I & 0 \\ X & 0 & 0 & 0 & -Q^{-1} \end{bmatrix} \begin{bmatrix} W_1 & 0 & 0 & 0 & 0 \\ 0 & I & 0 & 0 & 0 \\ 0 & 0 & I & 0 & 0 \\ 0 & 0 & 0 & I & 0 \\ 0 & 0 & 0 & 0 & I \end{bmatrix} < 0; \quad (7)$$

$$\begin{bmatrix} W_2 & 0 & 0 & 0 \\ 0 & W_2 & 0 & 0 \\ 0 & 0 & I & 0 \\ 0 & 0 & 0 & I \end{bmatrix}^T \begin{bmatrix} YA + A^T Y + Q & 0 & YB_1 & C_1^T \\ 0 & -(1-\rho)Q & 0 & 0 \\ B_1^T Y & 0 & -\gamma I & 0 \\ C_1 & 0 & 0 & -\gamma I \end{bmatrix} \begin{bmatrix} W_2 & 0 & 0 & 0 \\ 0 & W_2 & 0 & 0 \\ 0 & 0 & I & 0 \\ 0 & 0 & 0 & I \end{bmatrix} < 0; \quad (8)$$

$$\begin{bmatrix} X & I \\ I & Y \end{bmatrix} \geq 0; \quad (9)$$

Define:

$$\Phi = \begin{bmatrix} PA_0 + A_0^T P + E^T Q E & 0 & PB_0 & C_0^T \\ 0 & -(1-\rho)E^T Q E & 0 & 0 \\ B_0^T P & 0 & -\gamma I & 0 \\ C_0 & 0 & 0 & -\gamma I \end{bmatrix} \quad (10)$$

$$\Sigma = \begin{bmatrix} P & 0 & 0 & 0 \\ 0 & I & 0 & 0 \\ 0 & 0 & I & 0 \\ 0 & 0 & 0 & I \end{bmatrix}; \quad \Pi = \begin{bmatrix} B_{00} & B_x \\ 0 & 0 \\ 0 & 0 \\ 0 & 0 \end{bmatrix}; \quad \Theta = \begin{bmatrix} C_{00}^T & 0 \\ 0 & C_{00}^T \\ 0 & 0 \\ 0 & 0 \end{bmatrix} \quad (11)$$

$$F = (\Sigma \Pi)^T = \begin{bmatrix} F_1 \\ F_2 \end{bmatrix}; \quad G = \Theta^T = \begin{bmatrix} G_1 \\ G_2 \end{bmatrix}; \quad \tilde{K} = \begin{bmatrix} K & 0 \\ 0 & K \end{bmatrix} \quad (12)$$

$$\frac{\Phi}{2} + F_1^T K G_1 + F_2^T K G_2 < 0 \quad (13)$$

The meanings of all these symbols are described in Appendixs A and B.

4.4. Additional PID Control Module

While the H_∞ controller can improve the system dynamic performance as well as ensure the internal stability of the system with communication delays, it cannot eliminate the steady-state error. With regards to LFC, no matter whether the Flat Frequency Control mode (FFC), the Flat Tie-line Control mode (FTC) or the Tie line Bias Control mode (TBC) are used, the ultimate goal is to control a system dynamic index (Δf , ΔP_{tie} or ACE) to zero so that the system will go back to its original steady state operating point after being disturbed. To achieve this, we propose to add a PID control module into the controller. The methods for tuning PID parameters are highly developed (such as the proportion degree method and response curve method). By adding a PID component, we can improve the dynamic performance, reduce overshoot, accelerate the response speed and eliminate the steady-state error.

4.5. The Design Procedure of Suboptimal H_∞ -PID Output Feedback Control Method

Step 1. Linearize the system near the steady state operating point, and formulate the state-space equations in the form of (2).

Step 2. For a pre-given symmetric positive definite matrix Q (The unit matrix), obtain feasible solutions X, Y by solving LMIs (7)–(9).

Step 3. Obtain the full column rank matrices $M, N \in R_{n \times k}$ that satisfy the equation $MN^T = I - XY$, using the Singular Value Decomposition method.

Step 4. Calculate the linear equation $\begin{bmatrix} Y & I \\ N^T & 0 \end{bmatrix} = P \begin{bmatrix} I & X \\ 0 & M^T \end{bmatrix}$ to get the symmetric positive definite matrix P .

Step 5. From (10)–(12), obtain Φ, F_1, F_2, G_1, G_2 . Then solve LMI (13) to get controller's H_∞ part: K .

Step 6. Select appropriate signals as the input of the PID controller. Then tune the PID parameters to accelerate the response speed as well as to eliminate the steady-state error.

5. Case Studies

5.1. Studies on a Two-Area Test System

In order to verify the effectiveness of the proposed control method, a two-area LFC system derived from the New England 39-bus system is studied. The parameters of the LFC system are shown in Table 2.

The New England 39-bus test power system has 46 transmission lines and the topology is shown in Figure 5. Generator No. 1 is a wind generator, and there is one EV aggregator in each area that controls all the PEVs register to participate in frequency regulation. Buses 15 and 16 are low-voltage nodes, while the two lines that connect buses 14 and 15, 16 and 17 divide the whole system into 2 separate areas, i.e., the tie lines of the test system. The total capacity of the system is 6297.5 MW, and the load fluctuation in area-1 and area-2 are set to 300 MW and 200 MW separately (0.3 p.u. and 0.2 p.u. on 1000 MVA base). The required frequency regulation capacity is set to 8% of the total loads, namely 503.8 MW, in which the conventional AGC plants and electric vehicles account for 80% (407.0 MW) and 20% (100.8 MW) respectively. If each battery can at most provide 3 kW discharging power, then we need around 34,000 PEVs to register to take part in the ancillary service.

Table 2. Parameters' settings of the two-area LFC system studies.

Parameters	Values	
	Area 1	Area 2
Regional frequency deviation coefficient, k_{bi} (p.u. MW/Hz)	4.89	5.12
Speed regulation due to governor action, R_i (Hz/p.u. MW)	0.12	0.08
Inertia time constants of the AGC units, M_i (s)	6.23	5.77
Load frequency characteristic coefficient, D_i (p.u. MW/Hz)	0.87	1.23
Governor time constant, t_{gi} (s)	0.23	0.27
Turbine time constant, t_{chi} (s)	0.56	0.45
Capacity distribution coefficients for frequency regulation of units, k_{sgi}	0.80	0.70
Capacity distribution coefficients for frequency regulation of EVs, k_{sevi}	0.20	0.30
Frequency response coefficients of evs, k_{evi} (p.u. MV/Hz)	3.00	2.00
Equivalent time constant of batteries, t_{evi} (s)	0.12	0.20
Tie line synchronization coefficient, T_i (p.u. MV/Hz)	2.00	

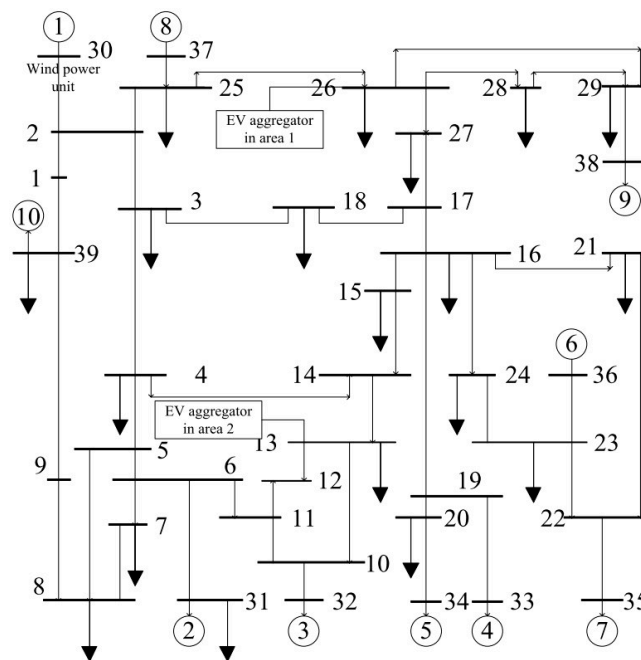


Figure 5. The network diagram of the IEEE 10-unit 39-bus two-area test system with EVs and wind power.

The two proposed control methods will be tested, here we choose seven states of the total nine ones as the feedbacks by excluding the valve opening degree of the AGC units in the two areas. For full-state feedback, H_∞ -PID controller parameters are:

$$K = \begin{bmatrix} -17.73 & -0.26 & -0.93 & -0.32 & -2.93 & 1.22 & -0.19 & -0.02 & 0.01 \\ -2.02 & -0.02 & -0.07 & -0.03 & -1.67 & -8.66 & -0.12 & -0.42 & -0.28 \end{bmatrix}$$

$$K_{p1} = 72.32; K_{I1} = 46.21; K_{D1} = 11.31$$

$$K_{p2} = 65.12; K_{I2} = 32.42; K_{D2} = 14.12$$

For output feedback, the dimension parameter is $n = 9; m = 2; q = 2; p = 2$. the H_∞ -PID controller parameters are:

$$A_K = \begin{bmatrix} -1015.220 & -1.214 & 3.173 & -3.754 & 0.052 & -0.052 & 0 & 0 & 0 \\ -1.202 & -1021.900 & 2.959 & 1.187 & 0.048 & 0.016 & 0 & 0 & 0 \\ 8.772 & 8.100 & 6.115 & 0.045 & 15.676 & -0.013 & 0.006 & 0.001 & 0 \\ -13.748 & 4.301 & 0.051 & 3.712 & 0.036 & 12.964 & -0.017 & 0 & 0 \\ -2.723 & -2.534 & -898.514 & -2.561 & -1514.903 & 0.406 & 0.015 & -0.047 & 0.007 \\ 3.195 & -1.005 & 0.580 & -889.387 & 0.625 & -1498.706 & -0.141 & -0.012 & -0.013 \\ -0.807 & 0 & -66.072 & 163.287 & 32.647 & -78.347 & -439.111 & 0.129 & 0.241 \\ -0.569 & -0.991 & -295.448 & -95.925 & 151.045 & 47.725 & 2.143 & -83.123 & -0.0245 \\ 1.641 & 0.114 & 158.343 & -286.452 & -81.203 & 144.496 & -9.315 & -1.113 & -31.500 \end{bmatrix}$$

$$D_K = \begin{bmatrix} 0.002 & -0.044 & -0.044 & 0 & 0 & 0 & 0 \\ 0 & 0 & 0 & 0 & 0.006 & -0.136 & -0.013 \end{bmatrix}$$

$$K_{p1} = 51.24; K_{I1} = 44.92; K_{D1} = 8.37$$

$$K_{p2} = 50.89; K_{I2} = 38.10; K_{D2} = 13.46$$

$$B_K = \begin{bmatrix} -0.010 & 0.018 & 6.476 & 0 & 0.007 & -0.014 & -3.950 \\ 0.005 & -0.005 & -3.968 & 0 & 0.010 & -0.013 & -6.583 \\ -0.002 & 0.015 & -0.025 & 0.065 & 0.545 & -4.098 & 0.087 \\ 0.510 & -4.173 & 0.105 & -0.139 & 0.008 & -0.022 & -0.026 \\ 0.191 & -1.088 & 0.001 & -8.539 & -19.851 & 395.178 & -0.024 \\ -29.297 & 480.408 & -0.034 & 23.935 & -1.273 & 1.409 & -0.004 \\ -275.138 & -69.540 & -0.447 & 1700.419 & -74.162 & 21.785 & -0.107 \\ 690.361 & 23.636 & 2.279 & 177.915 & 1634.886 & 48.606 & 5.994 \\ 1664.922 & 50.721 & 13.454 & 275.508 & -728.684 & -14.574 & -6.562 \end{bmatrix}; C_k = \begin{bmatrix} 0 & 0 \\ 0 & 0 \\ 0 & 0.002 \\ 0 & 0 \\ 0 & -0.252 \\ -0.010 & 0 \\ 0.006 & -0.009 \\ -0.003 & -0.021 \\ -0.006 & 0.008 \end{bmatrix}^T$$

Assume that the LFC mode is FFC, i.e., the control objective is to ensure the frequency deviation returns to zero after the disturbance. Set the load fluctuation vector $w(t) = [w_1 w_2]^T = [\Delta P_{L1} \Delta P_{L2}]^T = [0.3 \ 0.2] p.u.$, with a communication delay of 0.1 s. The system frequency deviations of the two areas, as well as the generators' outputs and the PEVs' power outputs are shown in Figure 6a,b respectively.

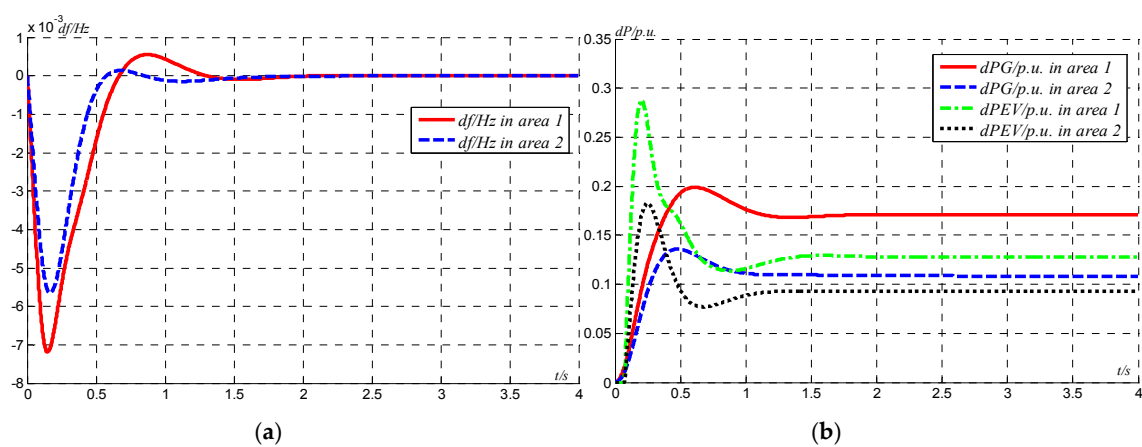


Figure 6. (a) The frequency derivation characteristics of the two-area system; (b) power outputs of generators and EVs.

It can be seen from Figure 6a that since the FFC control mode is applied, both the frequency deviation df in two areas can be adjusted to zero within 4.5 s. Moreover, it is evident from Figure 6b that the total load increase 0.5 p.u. is optimal and taken by generators and EVs in the end.

5.2. Comparison of Control Methods

With identical system parameters, studies are performed and comparison of the performances of different control methods, namely the traditional PI control, optimal H_∞ -PID full-state feedback control, and suboptimal H_∞ -PID output feedback control are carried out. Figure 7 shows the frequency deviations in area 1 in two scenarios, one with no delay (Figure 7a) and another with 0.5 s delay (Figure 7b).

It can be concluded from Figure 7a that when there is no delay in the network, all three control methods can guarantee the stability of the system, and the corresponding performance indexes are: (overshoot -0.00719 Hz, stabilization time 5.7 s) for PI control; (overshoot -0.00501 Hz, stabilization time 4.3 s) for full-state feedback control; (overshoot -0.00723 Hz, stabilization time 4.0 s) for output feedback control. Generally, optimal H_∞ -PID full-state feedback control outperforms its competitors, while the worst method is traditional PI control.

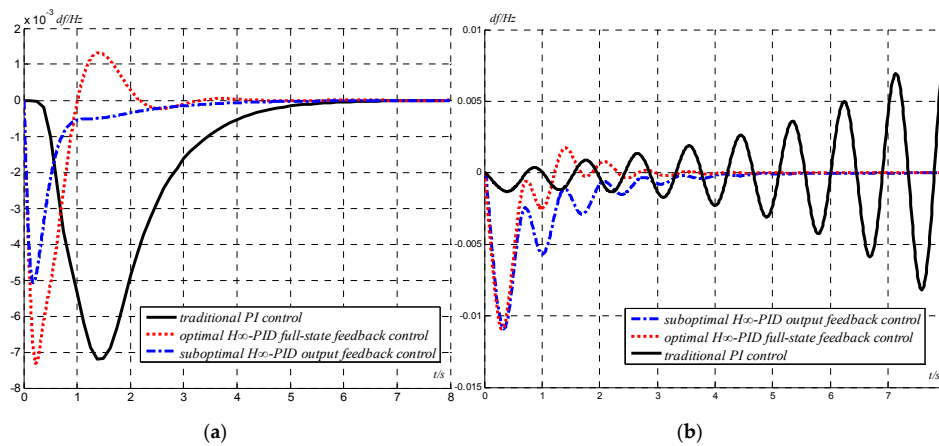


Figure 7. The frequency deviation in area 1: (a) no delay; (b) 0.5 s delay.

As the time delay increases to 0.5 s as shown in Figure 7b, the PI control loses its stability. However, the other two control methods still help the system to be robust stable. Therefore, the two control methods proposed in this paper are effective in maintaining the stability under communication delay conditions in a networked control channel.

5.3. Effects of Duration and Form of Communication Delay on System Dynamic Characteristics

To test the suboptimal H_∞ -PID output feedback controller further, all the parameters are the same except the delay settings are changed from 0 to 0.2 s and 0.4 s.

Figure 8a shows the variation of the system frequency deviation and Figure 8b shows the power output of AGC units and EVs in area 1 under different network delays. It can be seen from Figure 8 that although the system can eventually return to its steady operating point, the performance becomes worse as the delay increases. The relevant results are shown in Table 3.

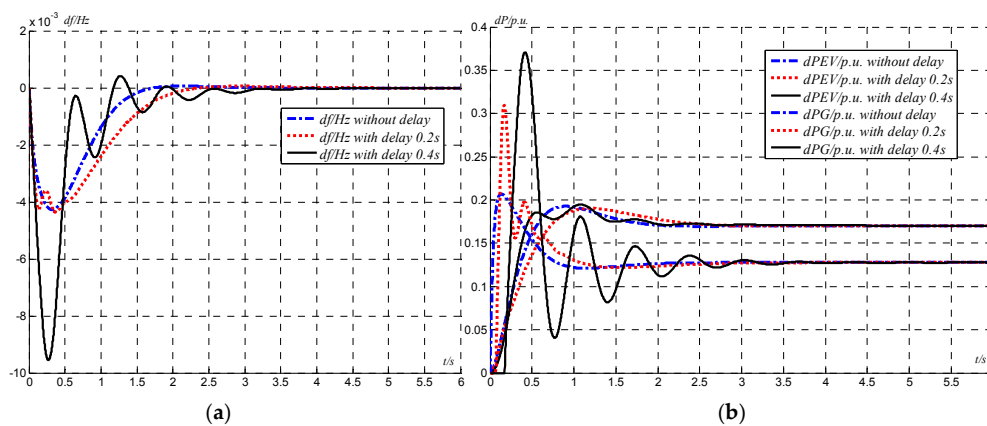


Figure 8. (a) System frequency deviation; (b) overall outputs of generators and EVs.

Table 3. Impacts of time delay on suboptimal H_∞ -PID control performance.

Performance		df/Hz	dP _G /p.u.	dP _{EV} /p.u.
Overshoot	$\tau = 0$	-4.2×10^{-3}	0.023	0.078
	$\tau = 0.2$ s	-4.3×10^{-3}	0.020	0.192
	$\tau = 0.4$ s	-9.7×10^{-3}	0.028	0.244
Stabilization Time (s)	$\tau = 0$	1.7	2.2	2.5
	$\tau = 0.2$ s	2.4	2.8	2.9
	$\tau = 0.4$ s	3.9	3.8	4.1

The negative impact can be quantified by the case when the time delay setting is changed from 0 s to 0.4 s. It can be observed from Table 3 that: (i) the overshoot of the frequency increases by 130.1%, and the stabilization time increases by 129.4%; (ii) the overshoot of the units output increases by 21.7%, and the stabilization time increases by 72.7%; and (iii) the overshoot of the EV output increases by 212.8%, and the stabilization time increases by 64.0%. The communication delay can be fixed or time-varying. Figure 9 shows the frequency curves under three different forms of delays.

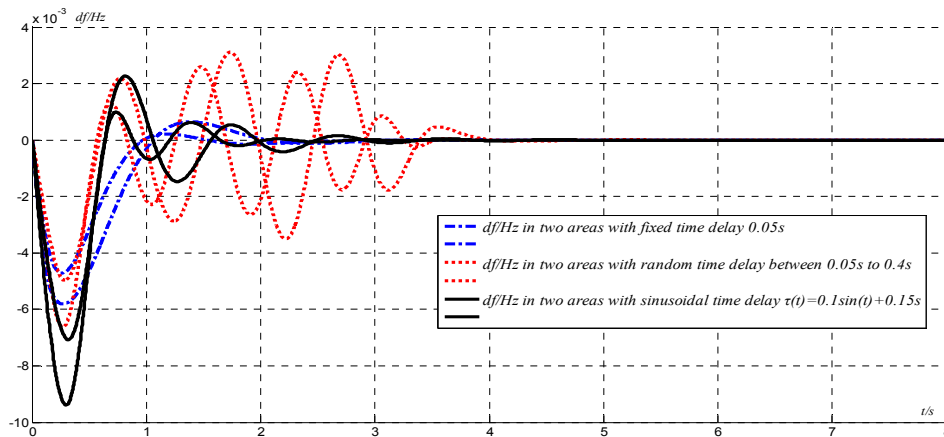


Figure 9. The system frequency deviation under different delays in two areas.

It can be seen that system dynamic responses varies with the different forms of delays. However, for all the cases, the proposed hybrid control method can ensure the system is robust stable no matter what form of delay is experienced.

5.4. Improvement of Dynamic Performance by EVs

The effect of EVs on system dynamic performance due to abrupt load variations is presented in this section. The suboptimal H_∞ -PID output feedback control is employed in this study and all system parameters remain intact. Figure 10a shows different frequency deviation characteristics, while Figure 10b shows power output deviations, with and without EVs under a step load change of 0.5 p.u. From Figure 10a,b, it can be seen that, with PEVs' participation, the overshoot and stabilization times are dramatically shorter. This demonstrates that with proper designed controllers, the dynamic performance of the whole system can be effectively enhanced by using PEVs for frequency regulation.

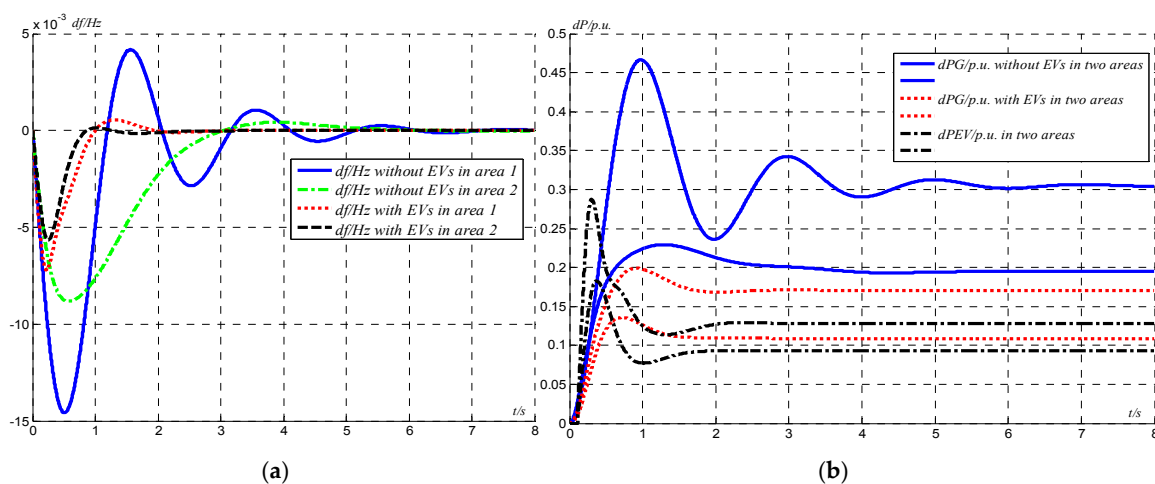


Figure 10. (a) The system frequency deviation; (b) the overall outputs of generators and EVs.

Besides, it can be seen that the AGC units take all the 0.5 p.u. load increment without the help of EVs, whereas with EVs participation, the total load increment has been optimally distributed between EVs and the AGC generators. Hence, EVs can reduce the required AGC capacity, the construction cost and the damage made to conventional generator units by avoiding the need for these units to make large changes abruptly in their output.

5.5. Effects of EVs on System Accommodation of Intermittent Wind Power

The following study assumes that the disturbances come from the uncertain wind power outputs. The random wind power output module is simulated with band-limited white noise and a low-pass filter [19]. The variations of system frequency in area 1 with and without the EVs' participation are shown in Figure 11.

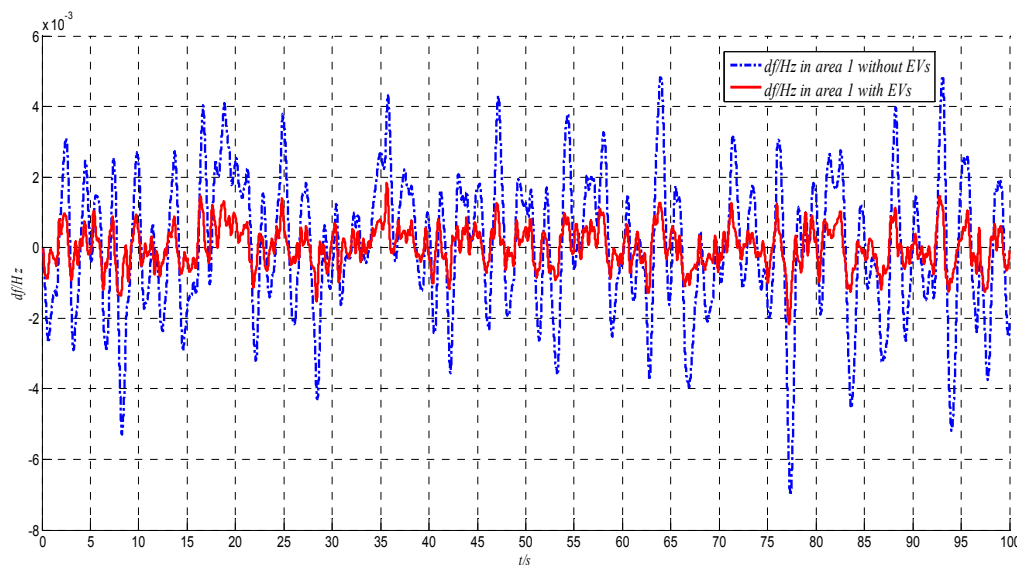


Figure 11. The system frequency deviation in area 1 under wind power fluctuations with and without EVs' participation.

From Figure 11, the fluctuation interval of the system frequency deviation without EVs is $[-0.00703, 0.00487]$ Hz which is greater than $[-0.00211, 0.00186]$ Hz with EVs. The EVs has reduced the overall fluctuation interval by 66.6%.

6. Conclusions

To enable a large fleet of idling electric vehicles to participate in the LFC process of a power system and at the same time take into account the communication delay between the control center and the PEVs, this paper has presented a framework of the networked frequency regulation for power systems with PEVs. Then a novel block diagram of the closed-loop LFC system with PEVs and wind power module has been proposed. Two novel control methods, based on rigorous mathematical analysis and LMI theory, have also been developed for system LFC to ensure the robustness and stability of the system taking into the effects of random disturbances and communication delay. The proposed optimal and sub-optimal H_∞ -PID controllers have been validated and they outperform the conventional PI controller. Whilst the full optimal H_∞ -PID method may not be fully practical and is subject to further advanced development in PMU, WAM and state estimation methods, the effectiveness of the proposed sub-optimal H_∞ -PID controller has been further demonstrated through appropriate case studies. These studies have also demonstrated that, under the control process given by the proposed sub-optimal H_∞ -PID controller, PEVs as energy storage devices can be significantly

beneficial to the overall power system frequency regulation even when the system contains intermittent wind power generation sources.

Acknowledgments: This work is jointly supported by the National Natural Science Foundation of China (No. 51477151), the National Basic Research Program (973 Program) (No. 2013CB228202), and a project from State Grid Zhejiang Electric Power Company (5211DF150007).

Author Contributions: Yunpeng Guo conceived the project, proposed the methodological framework and implementation roadmap; Liyan Zhang designed the implementation algorithm, performed the simulations; Junhua Zhao and Fushuan Wen organized the research team, reviewed and improved the methodological framework and implementation algorithm; Abdus Salam, Jianwei Mao, Liang Li reviewed and polished the manuscript. All authors discussed the simulation results and approved the assessment methodology.

Conflicts of Interest: The authors declare no conflict of interest.

Appendix A. Proof of the Theorem 1

Proof:

Lemma A1 [20]. For a system with time delay as described by

$$\begin{cases} \dot{x}(t) = Ax(t) + A_d x(t - \tau) + Bw(t) \\ z(t) = Cx(t) \end{cases} \quad (\text{A1})$$

and a pre-given constant γ , assume that the network delay $\tau(t)$ satisfies the condition $0 \leq \tau(t) < \infty$, $\dot{\tau}(t) \leq \rho < 1$ if there exist two positive definite matrixes P and Q such that the following LMI holds (<0 indicates the matrix is negative definite, $E = [I \ 0]$):

$$\begin{bmatrix} PA + A^T P + E^T Q E & P A_d & P B & C^T \\ A_d^T P & -(1 - \rho) E^T Q E & 0 & 0 \\ B^T P & 0 & -\gamma I & 0 \\ C & 0 & 0 & -\gamma I \end{bmatrix} < 0 \quad (\text{A2})$$

then the system is robustly stable, and the interference suppression degree index is γ . This lemma is—used to determine whether the designed system has the H_∞ performance.

Since $u(t) = Kx(t)$, so $u(t - \tau) = Kx(t - \tau)$. Put it into the Equation (2), we can attain:

$$\begin{cases} \dot{x}(t) = (A + B_2 K)x(t) + B_3 Kx(t - \tau) + B_1 w(t) \\ z(t) = C_1 x(t) \end{cases} \quad (\text{A3})$$

Based on the Lemma A1, one sufficient condition for ensuring the system described by (A3) is robust stabilized and has the interference suppression degree index γ is that there exist positive definite matrixes P and Q such that the following LMI holds:

$$\begin{bmatrix} (A + B_2 K)^T P + P(A + B_2 K) + E^T Q E & P B_3 K & P B_1 & C_1^T \\ (B_3 K)^T P & -(1 - \rho) E^T Q E & 0 & 0 \\ B_1^T P & 0 & -\gamma I & 0 \\ C_1 & 0 & 0 & -\gamma I \end{bmatrix} < 0 \quad (\text{A4})$$

By left multiplying and right multiplying the matrix:

$$\begin{bmatrix} P^{-1} & 0 & 0 & 0 \\ 0 & P^{-1} & 0 & 0 \\ 0 & 0 & I & 0 \\ 0 & 0 & 0 & I \end{bmatrix}$$

and simplifying the formulation, we can attain:

$$\begin{bmatrix} \Xi_1 & B_3KP^{-1} & B_1 & P^{-1}C_1^T \\ P^{-1}K^TB_3^T & -(1-\rho)P^{-1}E^TQEP^{-1} & 0 & 0 \\ B_1^T & 0 & -\gamma I & 0 \\ C_1P^{-1} & 0 & 0 & -\gamma I \end{bmatrix} < 0 \quad (\text{A5})$$

where, $\Xi_1 = P^{-1}(A + B_2K)^T + (A + B_2K)P^{-1} + P^{-1}E^TQEP^{-1}$.

Define $X = P^{-1}$, $Y = KP^{-1}$, $S = P^{-1}E^TQEP^{-1}$, then Equation (A5) can be changed as Equation (3). We can complete the proof.

Appendix B. Proof of the Theorem 2

Proof: After the linearization near the steady operating point of the system, the state-space equations can be derived through mathematical reasoning as (A6) shows:

$$\begin{cases} \dot{x}(t) = Ax(t) + B_2u(t) + B_3u(t - \tau) + B_1w(t) \\ z(t) = C_1x(t) \end{cases} \quad (\text{A6})$$

where,

$x = [x_1, x_2 \dots \dots x_n]^T \in R^{n \times 1}$ are n -dimension state variables;

$u = [u_1, u_2 \dots \dots u_m]^T \in R^{m \times 1}$ are m -dimension control variables;

$z = [z_1, z_2 \dots \dots z_p]^T \in R^{p \times 1}$ are p -dimension control output variables;

$w = [w_1w_2 \dots \dots w_q]^T \in R^{q \times 1}$ are q -dimension disturbance variables.

The rest are coefficient matrixes with suitable dimensions: $A \in R^{n \times n}$; $B_2 \in R^{n \times m}$; $B_3 \in R^{n \times m}$; $B_1 \in R^{n \times q}$; $C_1 \in R^{p \times n}$; if we choose measurable y as the dynamic output-feedback vector, the controller equations can be denoted as (4)–(6). Substituting Equation (4) into Equations (5)–(6) yields:

$$\begin{cases} \dot{\xi}(t) = A_k\xi(t) + B_kC_2x(t) \\ u(t) = C_k\xi(t) + D_kC_2x(t) \end{cases}$$

From Equation (A8), we can get:

$$u(t-\tau) = C_k\xi(t-\tau) + D_kC_2x(t-\tau) \quad (\text{A9})$$

Put (A8), (24) into (A6) and connect with (A7) we can get:

$$\begin{cases} \dot{x}(t) = Ax(t) + B_2C_k\xi(t) + B_2D_kC_2x(t) + B_3C_k\xi(t - \tau) + B_3D_kC_2x(t - \tau) + B_1w(t) \\ \dot{\xi}(t) = A_k\xi(t) + B_kC_2x(t) \\ z(t) = C_1x(t) \end{cases} \quad (\text{A10})$$

Introducing new symbols and writing the equations into matrix form, the closed-loop system can be expressed as:

$$\begin{cases} \dot{\bar{x}}(t) = \bar{A}\bar{x}(t) + \bar{A}_d\bar{x}(t - \tau) + \bar{B}w(t) \\ z(t) = \bar{C}\bar{x}(t) + \bar{D}w(t) \end{cases} \quad (\text{A11})$$

where, $\bar{x}(t) = \begin{bmatrix} x(t) \\ \zeta(t) \end{bmatrix} \in R^{(n+k) \times 1}$ are $(n+k)$ -dimension augmented state variables; the coefficient matrix can be denoted as:

$$\begin{cases} \bar{A} = \begin{bmatrix} A + B_2 D_k C_2 & B_2 C_k \\ B_k C_2 & A_k \end{bmatrix} \in R^{(n+k) \times (n+k)}; \\ \bar{A}_d = \begin{bmatrix} B_3 D_k C_2 & B_3 C_k \\ 0 & 0 \end{bmatrix} \in R^{(n+k) \times (n+k)}; \\ \bar{B} = \begin{bmatrix} B_1 \\ 0 \end{bmatrix} \in R^{(n+k) \times q}; \bar{C} = [C_1 \ 0] \in R^{p \times (n+k)}; \\ \bar{D} = [0] \in R^{p \times q}; \end{cases} \quad (\text{A12})$$

Then the problem can be changed as: for a pre-given positive constant γ , design a dynamic output feedback controller (4)–(6) to make the system described by (A6) robust stable and has the H_∞ performance γ . The controller is called a γ -suboptimal output feedback controller.

Apply the system described by (A10) into Lemma A1, we can get the robust stable conditions of the system is that the following LMI holds:

$$\begin{bmatrix} P\bar{A} + \bar{A}^T P + E^T Q E & P\bar{A}_d & P\bar{B} & \bar{C}^T \\ \bar{A}_d^T P & -(1-\rho)E^T Q E & 0 & 0 \\ \bar{B}^T P & 0 & -\gamma I & 0 \\ \bar{C} & 0 & 0 & -\gamma I \end{bmatrix} < 0 \quad (\text{A13})$$

Although it seems that the Equation (A13) gives one of the sufficient conditions that keeps the system robust stable, however, (A13) is an LMI with regards to all the unknown variables so that it is impossible to design a controller totally based on the formula above. So mathematical transformation has to be taken to change the form solvable.

Define the controller parameter matrix (to be designed) as $K = \begin{bmatrix} D_k & C_k \\ B_k & A_k \end{bmatrix} \in R^{(m+k) \times (l+k)}$, and then define the following matrixes:

$$\begin{cases} A_0 = \begin{bmatrix} A & 0 \\ 0 & 0 \end{bmatrix} \in R^{(n+k) \times (n+k)}; B_0 = \begin{bmatrix} B_1 \\ 0 \end{bmatrix} \in R^{(n+k) \times q}; \\ B_{00} = \begin{bmatrix} B_2 & 0 \\ 0 & I \end{bmatrix} \in R^{(n+k) \times (m+k)}; C_{00} = \begin{bmatrix} C_2 & 0 \\ 0 & I \end{bmatrix} \in R^{(l+k) \times (n+k)}; \\ B_x = \begin{bmatrix} B_3 & 0 \\ 0 & 0 \end{bmatrix} \in R^{(n+k) \times (m+k)}; C_0 = [C_1 \ 0] \in R^{p \times (n+k)}; \end{cases} \quad (\text{A14})$$

which only contains the known data of the model. Then the closed-loop system matrixes can be expressed as the affine functions of the controller parameters matrix K :

$$\begin{cases} \bar{A} = A_0 + B_{00} K C_{00} \\ \bar{A}_d = B_x K C_{00} \\ \bar{B} = B_0 \\ \bar{C} = C_0 \\ \bar{D} = [0] \in R^{p \times q} \end{cases} \quad (\text{A15})$$

Put Equation (A15) into Equation (A13), we can get:

$$\begin{bmatrix} \Omega & PB_xKC_{00} & PB_0 & C_0^T \\ C_{00}^TK^TB_x^TP & -(1-\rho)E^TQE & 0 & 0 \\ B_0^TP & 0 & -\gamma I & 0 \\ C_0 & 0 & 0 & -\gamma I \end{bmatrix} < 0 \quad (\text{A16})$$

where:

$$\Omega = P(A_0 + B_{00}KC_{00}) + (A_0^T + C_{00}^TK^TB_{00}^T)P + E^TQE$$

To continue simplify the controller, we have to expand the dimension of the controller to $\tilde{K} = \begin{bmatrix} K & 0 \\ 0 & K \end{bmatrix} \in R^{(2m+2k) \times (2l+2k)}$, then (A17) can be expressed as:

$$\Phi + (\Sigma\Pi)\tilde{K}\Theta^T + \Theta\tilde{K}^T(\Sigma\Pi)^T < 0 \quad (\text{A17})$$

where:

$$\Phi = \begin{bmatrix} PA_0 + A_0^TP + E^TQE & 0 & PB_0 & C_0^T \\ 0 & -(1-\rho)E^TQE & 0 & 0 \\ B_0^TP & 0 & -\gamma I & 0 \\ C_0 & 0 & 0 & -\gamma I \end{bmatrix} \in R^{(2n+2k+p+q) \times (2n+2k+p+q)} \quad (\text{A18})$$

$$\Sigma = \begin{bmatrix} P & 0 & 0 & 0 \\ 0 & I & 0 & 0 \\ 0 & 0 & I & 0 \\ 0 & 0 & 0 & I \end{bmatrix} \in R^{(2n+2k+p+q) \times (2n+2k+p+q)} \quad (\text{A19})$$

$$\Pi = \begin{bmatrix} B_{00} & B_x \\ 0 & 0 \\ 0 & 0 \\ 0 & 0 \end{bmatrix} \in R^{(2n+2k+p+q) \times (2m+2k)} \quad (\text{A20})$$

$$\Theta = \begin{bmatrix} C_{00}^T & 0 \\ 0 & C_{00}^T \\ 0 & 0 \\ 0 & 0 \end{bmatrix} \in R^{(2n+2k+p+q) \times (2l+2k)} \quad (\text{A21})$$

Lemma A2 (Projective Theorem) [21]. Assume that P, Q and H are pre-given appropriate dimension matrixes and H is symmetrical. N_P and N_Q are matrixes formed by any one set of the base vectors as column vectors from the nuclear space $\ker(P)$ and $\ker(Q)$ separately. Then there exists a matrix X such that

$$H + P^TX^TQ + Q^TXP < 0 \quad (\text{A22})$$

If and only if:

$$N_P^T H N_P < 0, N_Q^T H N_Q < 0 \quad (\text{A23})$$

Apply the Lemma A2 into (A17), we can obtain:

Formula is feasible with regards to \tilde{K} if and only if:

$$N_{\Pi}^T \Sigma^{-1} \Phi \Sigma^{-1} N_{\Pi} < 0 \quad (\text{A24})$$

$$N_{\Theta}^T \Phi N_{\Theta} < 0 \quad (\text{A25})$$

where N_{Π} and N_{Θ} are orthogonal complement matrixes of matrix Π and Θ separately. By applying Lemma A2, the inequalities in (A24) and (A25) no longer contain the unknown matrix variable \tilde{K} . Simplify (A24) and (A25) and express the Π and Θ in block forms separately as follows:

$$\Pi = \begin{bmatrix} B_2 & 0 & B_3 & 0 \\ 0 & I & 0 & 0 \\ 0 & 0 & 0 & 0 \\ 0 & 0 & 0 & 0 \\ 0 & 0 & 0 & 0 \end{bmatrix} \quad (\text{A26})$$

Take the orthogonal complement matrix $[W_1]$ of $[B_2 B_3]$, according to the definition of the orthogonal complement space, we can express N_{Π} as:

$$N_{\Pi} = \begin{bmatrix} W_1 & 0 & 0 & 0 \\ 0 & 0 & 0 & 0 \\ 0 & I & 0 & 0 \\ 0 & 0 & I & 0 \\ 0 & 0 & 0 & I \end{bmatrix} \quad (\text{A27})$$

In the same way:

$$\Theta = \begin{bmatrix} C_2^T & 0 & 0 & 0 \\ 0 & I & 0 & 0 \\ 0 & 0 & C_2^T & 0 \\ 0 & 0 & 0 & I \\ 0 & 0 & 0 & 0 \\ 0 & 0 & 0 & 0 \end{bmatrix} \quad (\text{A28})$$

Take the orthogonal complement matrix $[W_2]$ of $[C_2]^T$, according to the definition of orthogonal complement space, we can express N_{Θ} as:

$$N_{\Theta} = \begin{bmatrix} W_2 & 0 & 0 & 0 \\ 0 & 0 & 0 & 0 \\ 0 & W_2 & 0 & 0 \\ 0 & 0 & 0 & 0 \\ 0 & 0 & I & 0 \\ 0 & 0 & 0 & I \end{bmatrix} \quad (\text{A29})$$

Through matrix partition method, we can express the matrix P and its inverse matrix P^{-1} as:

$$P = \begin{bmatrix} Y & N \\ N^T & V \end{bmatrix}; P^{-1} = \begin{bmatrix} X & M \\ M^T & J \end{bmatrix} \quad (\text{A30})$$

Since P is symmetric, positive and definite, so $Y = Y^T \in R^{n \times n}$; $X = X^T \in R^{n \times n}$; $N \in R^{n \times k}$; $M \in R^{n \times k}$; $V \in R^{k \times k}$; $J \in R^{k \times k}$. If we put (A14), (A18), (A19), (A30) into (A31), and let $\Phi' = \Sigma^{-1} \Phi \Sigma^{-1}$, we can obtain:

$$\Phi' = \begin{bmatrix} AX + XA^T + XQX & AM + XQM & 0 & 0 & B_1 & XC_1^T \\ M^T A^T + M^T QX & M^T QM & 0 & 0 & 0 & M^T C_1^T \\ 0 & 0 & -(1-\rho)Q & 0 & 0 & 0 \\ 0 & 0 & 0 & 0 & 0 & 0 \\ B_1^T & 0 & 0 & 0 & -\gamma I & 0 \\ C_1 X & C_1 M & 0 & 0 & 0 & -\gamma I \end{bmatrix} \quad (A31)$$

Put (A27), (A31) into (A24) and then observe (A31) to delete the all-zero redundancy rows when doing the matrix multiplication. Finally, (A24) can be expressed as:

$$\begin{bmatrix} W_1 & 0 & 0 & 0 \\ 0 & I & 0 & 0 \\ 0 & 0 & I & 0 \\ 0 & 0 & 0 & I \end{bmatrix}^T \begin{bmatrix} AX + XA^T + XQX & 0 & B_1 & XC_1^T \\ 0 & -(1-\rho)Q & 0 & 0 \\ B_1^T & 0 & -\gamma I & 0 \\ C_1 X & 0 & 0 & -\gamma I \end{bmatrix} \begin{bmatrix} W_1 & 0 & 0 & 0 \\ 0 & I & 0 & 0 \\ 0 & 0 & I & 0 \\ 0 & 0 & 0 & I \end{bmatrix} < 0 \quad (A32)$$

Lemma A3 (Schur Theorem) [21]. Given the symmetric matrix $S \in R^{n \times n}$:

$S = \begin{bmatrix} S_{11} & S_{12} \\ S_{21} & S_{22} \end{bmatrix}$, in which the $S_{11} \in R^{r \times r}$, $S_{12} \in R^{r \times (n-r)}$, $S_{21} \in R^{(n-r) \times r}$, $S_{22} \in R^{(n-r) \times (n-r)}$, then the following three conditions are equivalent:

- (1) $S < 0$;
- (2) $S_{11} < 0, S_{22} - S_{12}^T S_{11}^{-1} S_{12} < 0$;
- (3) $S_{22} < 0, S_{11} - S_{12} S_{22}^{-1} S_{12}^T < 0$.

Since $S > 0$ and using Lemma A3, (A32) is equivalent with:

$$\begin{bmatrix} W_1 & 0 & 0 & 0 & 0 \\ 0 & I & 0 & 0 & 0 \\ 0 & 0 & I & 0 & 0 \\ 0 & 0 & 0 & I & 0 \\ 0 & 0 & 0 & 0 & I \end{bmatrix}^T \begin{bmatrix} AX + XA^T & 0 & B_1 & XC_1^T & X \\ 0 & -(1-\rho)Q & 0 & 0 & 0 \\ B_1^T & 0 & -\gamma I & 0 & 0 \\ C_1 X & 0 & 0 & -\gamma I & 0 \\ X & 0 & 0 & 0 & -Q^{-1} \end{bmatrix} \begin{bmatrix} W_1 & 0 & 0 & 0 & 0 \\ 0 & I & 0 & 0 & 0 \\ 0 & 0 & I & 0 & 0 \\ 0 & 0 & 0 & I & 0 \\ 0 & 0 & 0 & 0 & I \end{bmatrix} < 0 \quad (A33)$$

In the same way, put (27), (31), (42), (43) into (38), and then delete the all-zero redundancy rows when doing the matrix multiplication. Finally, we can get:

$$\begin{bmatrix} W_2 & 0 & 0 & 0 \\ 0 & W_2 & 0 & 0 \\ 0 & 0 & I & 0 \\ 0 & 0 & 0 & I \end{bmatrix}^T \begin{bmatrix} YA + A^T Y + Q & 0 & YB_1 & C_1^T \\ 0 & -(1-\rho)Q & 0 & 0 \\ B_1^T Y & 0 & -\gamma I & 0 \\ C_1 & 0 & 0 & -\gamma I \end{bmatrix} \begin{bmatrix} W_2 & 0 & 0 & 0 \\ 0 & W_2 & 0 & 0 \\ 0 & 0 & I & 0 \\ 0 & 0 & 0 & I \end{bmatrix} < 0 \quad (A34)$$

In conclusion, consider the system described by (19) and the given positive constant γ , if for the given symmetric positive definite matrix Q , there exists symmetric positive definite matrices X and Y that satisfy (46) and (47) as well as:

$$\begin{bmatrix} X & I \\ I & Y \end{bmatrix} \geq 0 \quad (A35)$$

Then there exists a γ -suboptimal output feedback H_∞ controller for system described by (A6). Where Equations (A33)–(A35) are simultaneous LMI equations that can be solved by the Matlab LMI toolbox.

The final problem is how to obtain P with X and Y , i.e., how to calculate K after getting Φ , $(\Sigma\Pi)$ and Θ . From Equation (A17) we can find that in which $\tilde{K} = \begin{bmatrix} K & 0 \\ 0 & K \end{bmatrix}$ is a special diagonal matrix

that cannot be solved directly using the Basiclmi function in the LMI-toolbox, hence the mathematical processing is needed as follows:

Define:

$$F = (\Sigma\Pi)^T = \begin{bmatrix} F_1 \\ F_2 \end{bmatrix}; G = \Theta^T = \begin{bmatrix} G_1 \\ G_2 \end{bmatrix}; \tilde{K} = \begin{bmatrix} K & 0 \\ 0 & K \end{bmatrix} \quad (\text{A36})$$

Put it into (A13), we can obtain:

$$\Phi + F_1^T K G_1 + F_2^T K G_2 + G_1^T K^T F_1 + G_2^T K^T F_2 < 0 \quad (\text{A37})$$

Equation (A31) can be divided into two parts, so we can get one of the sufficient conditions that makes (A31) holds:

$$\frac{\Phi}{2} + F_1^T K G_1 + F_2^T K G_2 < 0 \quad (\text{A38})$$

$$\frac{\Phi}{2} + G_1^T K^T F_1 + G_2^T K^T F_2 < 0 \quad (\text{A39})$$

Equations (A38) and (A39) are mutually transposed. As the transposition of the matrix does not change the polarity of the eigenvalues, so we can only solve (51) or (52) to get K that guarantees both LMIs hold. The dimension of the obtained γ -suboptimal output feedback H_∞ controller depends on the dimension of matrix P , while the dimension of matrix P depends on the dimension of $I-XY$. Therefore, after getting a feasible solution X and Y , we can use $\text{Rank}(I-XY) = k < n$ to define the dimension k . The proof is then completed.

References

1. Kempton, W.; Tomić, J. Vehicle-to-grid power implementation: From stabilizing the grid to supporting large-scale renewable energy. *J. Power Sources* **2005**, *144*, 280–294. [CrossRef]
2. Kempton, W.; Udo, V.; Huber, K.; Komara, K.; Letendre, S.; Baker, S.; Pearre, N. A Test of Vehicle-to-Grid (V2G) for Energy Storage and Frequency Regulation in the PJM System. Available online: <http://www.udel.edu/V2G/resources/test-v2g-in-pjm-jan09.pdf> (accessed on 25 January 2017).
3. Qian, K.J.; Zhou, C.K.; Allan, M.; Yuan, Y. Modeling of load demand due to EV battery charging in distribution systems. *IEEE Trans. Power Syst.* **2011**, *26*, 802–810. [CrossRef]
4. Hajimiragha, A.H.; Canizares, C.A.; Fowler, M.W.; Moazeni, S.; Elkamel, A. A robust optimization approach for planning the transition to plug-in hybrid electric vehicles. *IEEE Trans. Power Syst.* **2011**, *26*, 2264–2274. [CrossRef]
5. Wu, C.X.; Wen, F.S.; Lou, Y.L.; Xin, F. Probabilistic load flow analysis of photovoltaic generation systems with plug-in electric vehicles. *Int. J. Electr. Power Energy Syst.* **2015**, *64*, 1221–1228. [CrossRef]
6. Masuta, T.; Yokoyama, A. Supplementary load frequency control by use of a number of both electric vehicles and heat pump water heaters. *IEEE Trans. Smart Grid* **2012**, *3*, 1253–1262. [CrossRef]
7. Singh, M.; Kumar, P.; Kar, I. Implementation of vehicle to grid infrastructure using fuzzy logic controller. *IEEE Trans. Smart Grid* **2012**, *3*, 565–577. [CrossRef]
8. Sundstrom, O.; Binding, C. Flexible charging optimization for electric vehicles considering distribution grid constraints. *IEEE Trans. Smart Grid* **2012**, *3*, 26–37. [CrossRef]
9. Galus, M.D.; Koch, S.; Andersson, G. Provision of load frequency control by PHEVs, controllable loads and a cogeneration unit. *IEEE Trans. Ind. Electron.* **2011**, *58*, 4568–4582. [CrossRef]
10. Yodyium, T.; Mo-Yuen, C. Control methodologies in networked control systems. *Control Eng. Pract.* **2003**, *11*, 1099–1111.
11. Cloosterman, M.B.G.; Van de Wouw, N.; Heemels, W.P.M.H.; Nijmeijer, H. Stability of networked control systems with uncertain time-varying delays. *IEEE Trans. Autom. Control* **2001**, *21*, 84–89. [CrossRef]
12. Mullen, S.K. Plug-In Hybrid Electric Vehicles as a Source of Distributed Frequency Regulation. Ph.D. Thesis, University of Minnesota, Minneapolis, MN, USA, 2009.
13. Yao, W.F.; Zhao, J.H.; Wen, F.S.; Xue, Y.S.; Ledwich, G. A hierarchical decomposition approach for coordinated dispatch of plug-in electric vehicles. *IEEE Trans. Power Syst.* **2013**, *28*, 2768–2778. [CrossRef]

14. Wang, G.B.; Zhao, J.H.; Wen, F.S.; Xue, Y.S.; Ledwich, G. Dispatch strategy of PHEVs to mitigate selected patterns of seasonally varying outputs from renewable generation. *IEEE Trans. Smart Grid* **2015**, *6*, 627–639. [[CrossRef](#)]
15. Lu, C.F.; Liu, C.C.; Wu, C.J. Dynamic modeling of battery energy storage system and application to power system stability. *Proc. Inst. Elect. Eng. Gen. Transm. Distrib.* **1995**, *142*, 429–435. [[CrossRef](#)]
16. Jia, Y.M. *Robust H_∞ Control*; Science Press: Beijing, China, 2007.
17. Francis, B.; Zames, G. On H_∞ -optimal sensitivity theory for SISO feedback systems. *IEEE Trans. Autom. Control* **1984**, *29*, 9–16. [[CrossRef](#)]
18. Xia, Y.Q.; Jia, Y.M. Robust sliding mode control for uncertain time-delay systems: An LMI approach. *IEEE Trans. Autom. Control* **2003**, *48*, 1086–1092.
19. Takagi, M.; Yamaji, K.; Yamamoto, H. Power system stabilization by charging power management of plug-in hybrid electric vehicles with LFC signal. In Proceedings of the Vehicle Power and Propulsion Conference, Tokyo, Japan, 7–10 September 2009.
20. Jeung, E.T.; Kim, J.H.; Park, H.B. H_∞ -output feedback controller design for linear system with time-varying delayed state. *IEEE Trans. Autom. Control* **1998**, *43*, 971–974. [[CrossRef](#)]
21. Yu, L. *Robust Control: LMI Approach*; Tsinghua University Press: Beijing, China, 2002.



© 2017 by the authors. Licensee MDPI, Basel, Switzerland. This article is an open access article distributed under the terms and conditions of the Creative Commons Attribution (CC BY) license (<http://creativecommons.org/licenses/by/4.0/>).